Journal of Solid State Chemistry 181 (2008) 2325–2331

Contents lists available at ScienceDirect

Journal of Solid State Chemistry

journal homepage: www.elsevier.com/locate/jssc

Synthesis, structure and magnetic properties of $A_2MnB'O_6$ (A = Ca, Sr; B' = Sb, Ta) double perovskites

Tapas Kumar Mandal [a], Viktor V. Poltavets [a], Mark Croft [b], Martha Greenblatt [a,*]

[a] Department of Chemistry and Chemical Biology, Rutgers, The State University of New Jersey, 610 Taylor Road, Piscataway, NJ 08854, USA
[b] Department of Physics and Astronomy, Rutgers, The State University of New Jersey, 136 Frelinghuysen Road, Piscataway, NJ 08854, USA

ARTICLE INFO

Article history:
Received 5 February 2008
Received in revised form
22 April 2008
Accepted 26 April 2008
Available online 9 May 2008

Keywords:
Oxide
X-ray diffraction
Crystal structure
Magnetic properties
X-ray absorption spectroscopy (XAS)

ABSTRACT

$A_2MnB'O_6$ (A = Ca, Sr; B = Sb, Ta) double perovskites have been synthesized and their structural and magnetic properties have been investigated. Rietveld refinement of the powder X-ray diffraction data for Sr_2MnSbO_6 indicated significant ordering of Mn and Sb at the B-site while all other phases showed mostly a random distribution of the B-site cations. X-ray absorption spectroscopic data established the presence of Mn in the 3+ and Sb/Ta in the 5+ oxidation states in all the phases. Magnetic susceptibility data indicated ferromagnetic correlations for all the $A_2MnB'O_6$ phases with Weiss temperatures varying from 64 to 107 K.

1. Introduction

Double perovskite oxides ($A_2BB'O_6$) continue to attract research interest, because of their unique electrical and magnetic properties that include metallic/half-metallic ferri-/ferromagnetism and magnetoresistance effects [1]. Ordering of the transition metal ions (B and B') at the B-site of the perovskite structure plays a crucial role in determining their properties [2]. Although, it has been established that the size and charge difference between the B and B' cations facilitate ordering at the B-site [2], other factors, such as, specific bonding interactions (e. g. Jahn–Teller distortions and polarization properties) and also the synthesis condition and formation temperature may affect the degree of order [3].

The arrangement of B and B' cations in $A_2BB'O_6$ double perovskites may be rock salt- or layered-type [2]. While in rock salt-type ordering the B and B' cations order alternately in all three crystallographic directions, in a layered ordering, the layers of B and B' cations alternate along one of the crystallographic direction. Rock salt-type ordering is very common among double perovskites and gives rise to diverse materials properties. For example, A_2FeMoO_6 and A_2FeReO_6 (A = Ca, Sr, Ba) are known to be ferri/ferromagnetic with critical temperatures, T_c's in the range ~330–420 K [4]. Room-temperature magnetoresistance has been observed for Sr_2FeMoO_6 and Sr_2FeReO_6 due to intergrain tunneling [1f,1h,5]. The double perovskite family has been extensively revisited since the discovery of room-temperature half-metallicity and tunneling-type magnetoresistance effect in Sr_2FeMoO_6 and Sr_2FeReO_6. Moreover, the recent discovery of magnetocapacitance and magnetoresistance (*magnetodielectric effect*) near room temperature in a ferromagnetic semiconductor, La_2NiMnO_6 [6], has driven the field for further research to find exotic and useful materials properties.

Recently, there has been renewed interest in Sr_2MnSbO_6 due to the observation of cation ordering in this material [7] prepared at lower temperatures than the temperature employed before, when the completely disordered structure was formed [8]. Also, the Ta analog, Sr_2MnTaO_6 [9] was previously reported to form in a double perovskite structure on the basis of electron and neutron diffraction studies. The oxygen content, the formal oxidation state of the cations and the physical properties of these phases have not been systematically reported before. Jansen et al. [10] investigated structural and magnetic properties of $CaSb_xMn_{1-x}O_3$ ($0.1 \leqslant x \leqslant 0.5$) solid solutions and indicated magnetic clustering in those compounds. We extended the investigation of $Sr_2MnB'O_6$ (B' = Sb, Ta) and Ca_2MnSbO_6 and that of a new member Ca_2MnTaO_6 to find the synthetic conditions for possible cation ordering, to determine the extent of ordering and the physical properties of these phases. We have found significant cation ordering only in Sr_2MnSbO_6; the other compounds indicate B-cation disorder in all our synthetic approaches. In this paper, we report results of the compositional, structural, magnetic and X-ray absorption spectroscopic (XAS) investigations of these double perovskites.

* Corresponding author. Fax: +1 732 445 5312.
E-mail address: martha@rutchem.rutgers.edu (M. Greenblatt).

0022-4596/$ - see front matter © 2008 Elsevier Inc. All rights reserved.
doi:10.1016/j.jssc.2008.04.038

2. Experimental

Polycrystalline samples of $A_2MnB'O_6$ (A = Ca, Sr; B' = Sb, Ta) were synthesized by solid-state reactions from high purity ($\geqslant$99.9% Aldrich, or Alfa Aesar) stoichiometric quantities of $CaCO_3/SrCO_3$, Mn_2O_3 and Sb_2O_3/Ta_2O_5. The starting materials were intimately ground and heated in air in a stepwise manner, over a period of 4–7 days reaching the highest temperature of 1350 °C, and at each step checked for phase purity and development of ordering reflections by powder X-ray diffraction (PXD). The mixtures were thoroughly reground at the intermediate steps between two heating cycles. All the samples were slow cooled from their highest reaction temperatures to room temperature to maximize the oxygen content in the samples. A sample of $La_3Ni_2TaO_9$ that has been used as a Ta^{5+} standard in XAS study was prepared following the literature procedure [11].

PXD patterns were recorded at room temperature on a Bruker D8-Advance diffractometer (in Bragg–Brentano geometry with Cu$K\alpha$ radiation, $\lambda = 1.5418$ Å) equipped with a SOL-X solid-state detector. For structure refinements, PXD data were collected in the angular range 10–120° in steps of 0.02° and with a step time of 9 s. The refinements of crystal structures were performed by the Rietveld method [12] with the FULLPROF program [13]. In all of the refinements neutral atom scattering lengths, that are already stored in internal tables of the program, were used.

Thermogravimetric analyses (TGA) were carried out with a TA Instruments 2050 thermal analyzer. Samples were heated at a rate of 5 °C/min to a final temperature of 900 °C and cooled down to room temperature under air, O_2 or 10% H_2–Ar mixture depending on the experimental runs performed.

Magnetization data were collected with a quantum design MPMS-XL superconducting quantum interference device (SQUID) magnetometer. Temperature-dependent magnetization data were recorded at various applied magnetic fields (H) in the temperature range $2 \leqslant T(\mathrm{K}) \leqslant 400$ after cooling the sample in zero magnetic field (zero-field cooled (ZFC)) and also while cooling in the presence of the field (field-cooled (FC)). Measurements of magnetization (M) as a function of H were made at 5, 50 and 300 K over the magnetic field ranges $-50 \leqslant H(\mathrm{kOe}) \leqslant 50$.

The Mn-K and Ta-L_3 XAS measurements were performed in the fluorescence and transmission mode on powdered samples on beam line X-19A at the Brookhaven National Synchrotron Light Source with methods discussed in Refs. [14,15]. N_2 gas was used in the ionization chambers for these edges. Briefly the procedure used is as follows. The incident and transmitted beam intensities were measured with ionization chambers and the fluorescence intensities with Canberra PIPS detectors. The absolute energy calibration was set to the elemental edge (first inflection point). The relative energy scale was maintained to better than ± 0.05 eV with the simultaneously run standards.

In view of the low energy and strong "white-line" (WL) s-to-p transition feature the Sb-L_1 edge was measured in the total-electron-yield mode [16] with He gas in both the ionization and electron yield chambers. Here the "white line" terminology is conventional and refers to an atomic-like dipole transition into empty states which typically manifests a sharply peaked near edge structure, which in prior years would leave a white-line-streak on photographic film. Such total-electron-yield measurements prevent finite sample thickness rounding out the WL feature, while still provide a bulk XAS spectrum [16]. Since a simultaneous standard was not possible in the total-electron-yield mode, an elemental standard, run before and after the sample, was used and the relative energy was ± 0.1 eV or better.

As is routinely done, the spectra had a linear background subtracted (determined over ~80 eV interval below the edge), and were normalized to unity absorption step height across the edge. Here an average of the data in ~50–200 eV range above the edge was used to set the normalization value.

3. Results and discussion

3.1. Synthesis and structure

Formation of single phase double perovskite oxides of compositions $A_2MnB'O_6$ (A = Ca, Sr; B' = Sb, Ta) was monitored by recording PXD patterns of the polycrystalline samples at each stage of the reaction and checked for superstructure reflections due to cation ordering. Our preliminary investigation on the ordering of Mn and Sb cations in Sr_2MnSbO_6 even with PXD data indicated varied degrees of cation ordering starting at 1100 °C,

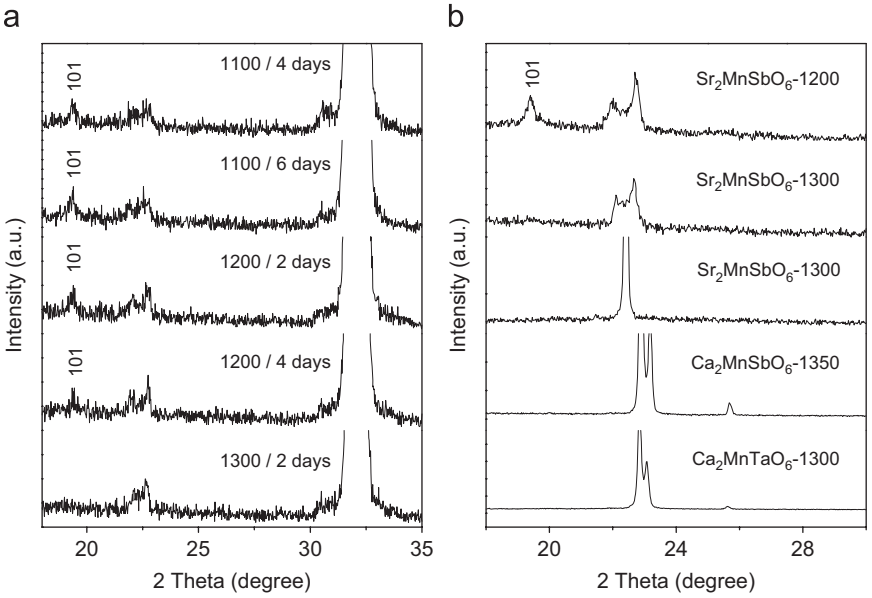

Fig. 1. PXD patterns of (a) Sr_2MnSbO_6 at various temperature and durations and (b) single-phase $A_2MnB'O_6$ (A = Ca, Sr; B' = Sb, Ta) at different temperatures in the two theta range 18–35°.

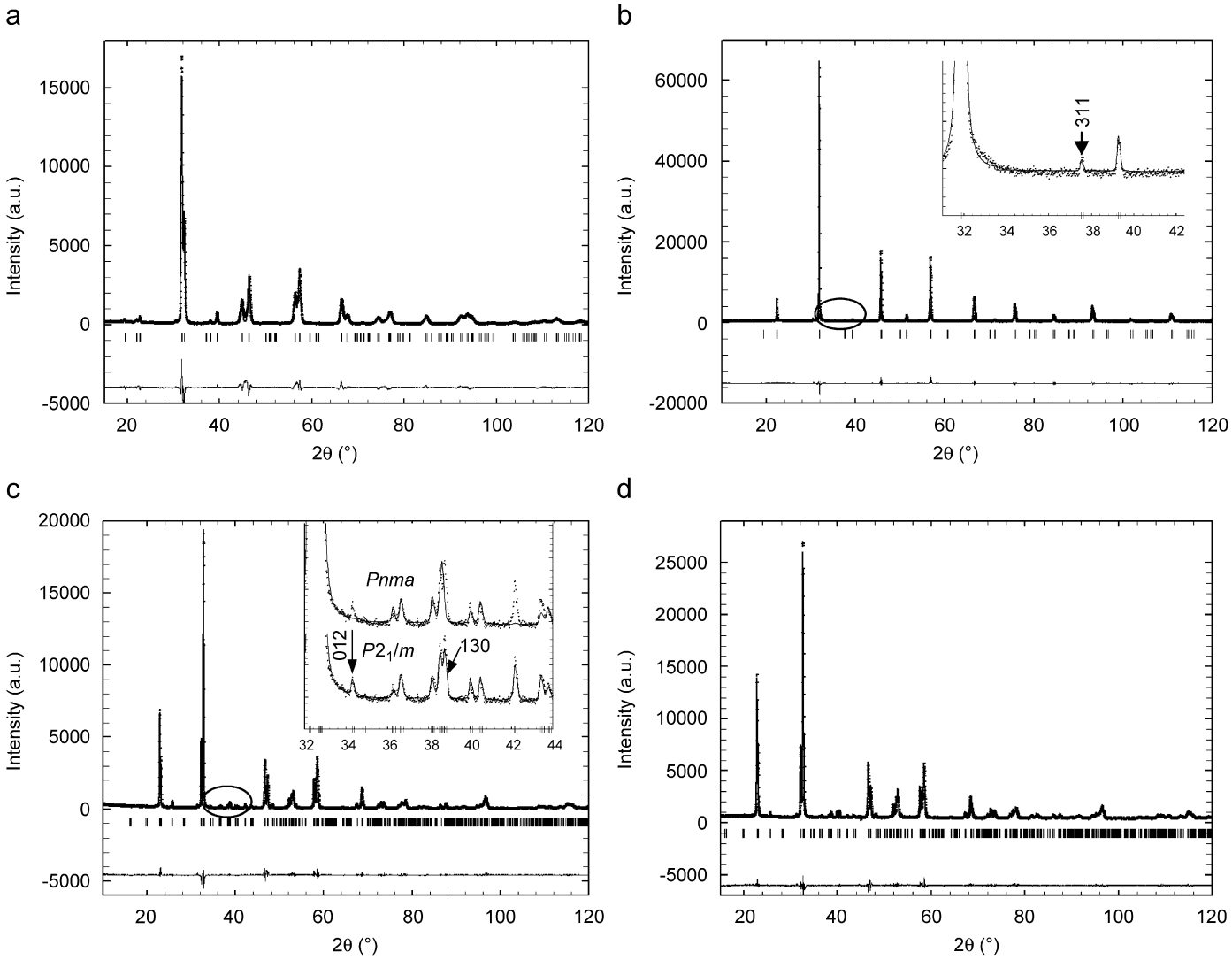

Fig. 2. Rietveld refinement of the structures of (a) Sr_2MnSbO_6, (b) Sr_2MnTaO_6, (c) Ca_2MnSbO_6 and (d) Ca_2MnTaO_6. Observed (+), calculated (line) and difference (bottom) profiles are shown. The vertical bars represent the Bragg positions. The inset in (b) shows an enlarged part of the profile indicating the 3 1 1 superstructure reflection and (c) shows a profile match comparison between *Pnma* and *P*21/*m* marking the 0 1 2 and 1 3 0 reflections.

which continue to persist up to 1200 °C. The ordering has been monitored with the emergence and intensity of the 1 0 1 reflection in the PXD data (Fig. 1a). A completely disordered Sr_2MnSbO_6 was obtained when the sample was heated at 1300 °C for 2 days (Fig. 1a). Rietveld refinements of the PXD data for Sr_2MnSbO_6 were carried out in space group *I*4/*m* after Kennedy et al. [8]. Samples prepared at 1200 °C/ for 2 days showed ~28% cation ordering as compared to ~20% for a higher annealing time (4 days) at the same temperature. Fig. 2 shows the Rietveld refinement profile for Sr_2MnSbO_6 synthesized at 1200 °C for 2 days and the refined atomic parameters along with occupancies and isotropic thermal factors are presented in Table 1.

In contrast to Sr_2MnSbO_6, our systematic investigation of other $A_2MnB'O_6$ (A = Ca, Sr; B' = Sb, Ta) phases mostly showed absence of cation ordering (Fig. 1b). A careful examination of the PXD patterns for Sr_2MnTaO_6 synthesized with a starting temperature of 900 °C and up to 1300 °C for various durations did not show significant manifestation of the ordering reflection similar to Sr_2MnSbO_6 indicative of *B*-site ordering. The Rietveld refinement of the structure of Sr_2MnTaO_6 has been carried out in *Fm*3*m* space group with a random distribution of Mn and Ta at the *B*-site. Moreover, the *R*-factors of the refinement in the *Pm*3*m* space group ($R_p = 5.2\%$ and $R_{wp} = 6.7\%$) with the simple perovskite structure were very similar to those in *Fm*3*m* space group ($R_p = 5.1\%$ and $R_{wp} = 6.6\%$). Refinement of the occupancies in *Fm*3*m*, however, indicated a slight preference (~5%) for Mn and Ta at the 4*a* and 4*b* sites, respectively. The refinement profile for Sr_2MnTaO_6 is shown in Fig. 2b and the refined atomic parameters are presented in Table 1. Our results are largely in agreement with those reported by Valldor et al. [9]. In the inset of Fig. 2b the enlarged portion of the profile shows the presence of (311) superstructure reflection, which supports space group *Fm*3*m* with a double perovskite structure. The fact that the peak intensity difference between the 111 and 311 superstructure reflections decreases with decreasing degree of ordering and approaching nearly equal intensity with a high degree of disorder (as obtained by simulating the Sr_2MnTaO_6 pattern with varying degree of order) and absence of a distinct 111 reflection in this case, could however be related to a higher and diffuse background in the low two theta around the 2 0 0 peak region. The substantial order of Mn/Sb compared to the near complete disorder of Mn/Ta may be attributed to the significantly larger difference in the effective ionic radii of Mn^{3+}–Sb^{5+} (Δr_{ionic} ~0.05 Å) [17] compared to Mn^{3+}–Ta^{5+} (Δr_{ionic}~0.01 Å).

Table 1
Lattice parameters, atomic positions and isothermal temperature factors for Sr_2MnSbO_6 and Sr_2MnTaO_6 double perovskites

Atom	Wyckoff	x	y	z	B_{iso}(Å^2)	Occ.
Sr_2MnSbO_6 (ordered), space group I4/m, a = 5.5419(3), c = 8.0947(5)Å; R_p = 10.1%, R_{wp} = 14.1% and R_B = 4.9%						
Sr	4*d*	0	0.5	0.25	0.35(4)	1.0
Mn1/Sb1	2*a*	0	0	0	0.10[a]	0.64(1)/0.36(1)
Mn2/Sb2	2*b*	0	0	0.5	0.10[a]	0.36(1)/0.64(1)
O1	4*e*	0	0	0.249(2)	1.04(27)	1.0
O2	8*h*	0.785(1)	0.725(3)	0	0.68(17)	1.0
Sr_2MnTaO_6, space group Fm3m, a = 7.9431(1)Å; R_p = 5.1%, R_{wp} = 6.6% and R_B = 5.1%						
Sr	8*c*	0.25	0.25	0.25	0.97(2)	1.0
Mn1/Ta1	4*a*	0	0	0	0.33(3)	0.54(1)/0.46(1)
Mn2/Ta2	4*b*	0.5	0.5	0.5	0.10[a]	0.46(1)/0.54(1)
O	24*e*	0.247(2)	0	0	0.83(9)	1.0

[a] Parameter was fixed at this value.

Formation of single phase materials for the Ca-analogs was achieved only at a temperature of 1300 °C and higher. Single phase Ca_2MnSbO_6 was obtained only at 1350 °C; below this temperature it was always contaminated with an admixture of $Ca_2Sb_2O_7$ pyrochlore phase. Rietveld refinement of the structure of Ca_2MnSbO_6 was carried out in space group *Pnma* ($R_p = 10.9\%$, $R_{wp} = 15.5\%$, $R_B = 8.4\%$ and $\chi^2 = 6.2$) as used by Lufaso et al. [7] with a disordered Mn/Sb arrangement and $a^+b^-b^-$ octahedral tilting according to Glazer's notation [18]. However, the profile description was inadequate in *Pnma* since all the observed reflections could not be indexed (e.g. 0 1 2 and 1 3 0; in *Pnma* only *k l with k+l = 2n and h k 0 for h = 2n are allowed [19]), and additional peak splitting was noted. Moreover, Mn/Sb ordering within the same tilt system would allow $P2_1/n$ symmetry, but was discarded due to absence of superstructure reflections required for cation ordering. Therefore, we have considered $P2_1/m$ with the $a^+b^-c^-$ tilt system as a possible space group, the only other monoclinic space group possible based on octahedral tilting distortions with cation disorder and the group–subgroup relationship schemes of octahedral tilting in perovskites [20,21]. The refinement of the structure of Ca_2MnSbO_6 in $P2_1/m$ ($R_p = 7.9\%$, $R_{wp} = 10.9\%$, $R_B = 5.3\%$ and $\chi^2 = 3.0$) (also used by Jansen et al. [10] with a random distribution of Mn and Sb at the 2b and 2c sites) gave a satisfactory description of the profile with indexing of all the reflections. The refinement profile is shown in Fig. 2c and the refined atomic parameters along with occupancies and isotropic thermal factors are given in Table 2. An enlarged part of the profile is shown in the inset of Fig. 2c to compare the adequate profile fit in $P2_1/m$ over Pnma.*

Synthesis of Ca_2MnTaO_6 was carried out in a stepwise manner and kept at each temperature for 48–96 h to reach the equilibrium condition. A single phase compound similar to Ca_2MnSbO_6 was obtained at 1300 °C without $Ca_2Ta_2O_7$ pyrochlore admixture. A close inspection of the PXD patterns after each heating did not indicate any sign of cation ordering for this phase as well. Therefore, the refinement of the PXD data was carried out in the same monoclinic $P2_1/m$ space group as used for the Sb analog. A satisfactory fit for the structure of Ca_2MnTaO_6 was obtained with the monoclinically distorted structure with zero cation ordering in the $a^+b^-c^-$ tilt system. The refinement profile is shown in Fig. 2d and the refined parameters are presented in Table 2.

Table 2
Atomic positions and isothermal temperature factors for $Ca_2MnB'O_6$ (B' = Sb, Ta)[a] double perovskites

Atom	Position	x	y	z	B_{iso} (Å^2)	Occ.
Ca1	2*e*	0.007(1)	0.25	−0.046(1)	2.0(2)	1.0
		0.017(2)	0.25	−0.039(2)	0.5(3)	1.0
Ca2	2*e*	0.484(1)	0.25	0.456(1)	0.2(1)	1.0
		0.496(2)	0.25	0.452(2)	1.8(4)	1.0
Mn	2*b*	0.5	0	0	0.3(1)	0.5
		0.5	0	0	0.1[b]	0.5
B′	2*c*	0	0	0.5	0.1(1)	0.5
		0	0	0.5	0.1[b]	0.5
O1	2*e*	−0.108(3)	0.25	0.555(2)	0.9(1)	1.0
		−0.072(5)	0.25	0.541(3)	0.2(1)	1.0
O2	2*e*	0.565(3)	0.25	0.004(3)	1.1(1)	1.0
		0.603(5)	0.25	0.015(4)	0.2(1)	1.0
O3	4*f*	0.208(2)	0.051(2)	0.217(3)	1.1(1)	1.0
		0.208(3)	0.024(2)	0.209(3)	0.2(1)	1.0
O4	4*f*	0.304(2)	0.039(2)	0.704(3)	1.0(1)	1.0
		0.297(3)	0.059(2)	0.698(3)	0.2(1)	1.0

[a] Top row, Ca_2MnSbO_6, space group $P2_1/m$, $a = 5.4607(1)$, $b = 7.6934(1)$, $c = 5.5548(1)$ Å and $\beta = 90.134(2)^\circ$; $R_p = 7.9\%$, $R_{wp} = 10.9\%$ and $R_B = 5.3\%$. Bottom row, Ca_2MnTaO_6, space group $P2_1/m$, $a = 5.4600(1)$, $b = 7.7200(1)$, $c = 5.5674(1)$ Å and $\beta = 90.078(3)^\circ$; $R_p = 4.2\%$, $R_{wp} = 5.5\%$ and $R_B = 3.8\%$.
[b] Parameter was fixed at this value.

3.2. X-ray absorption spectra

The Mn-*K* edges of $A_2MnB'O_6$ (A = Ca, Sr; B' = Sb, Ta) along with other standard compounds are shown in Fig. 3a. The Mn-*K* edges of $A_2MnB'O_6$ has been compared with other octahedrally coordinated standards, namely, MnO with NaCl-structure and a series of Mn-containing compounds with simple perovskites as well as double perovskite structures. The chemical shift of all the $A_2MnB'O_6$ compounds appears highly consistent with the assignment of a Mn^{3+} valence state.

As a *p*-block element the frontier bonding orbital of Sb are the 5*p*-states with the 5*s*-states being involved in the higher valance state. The Sb-L_1 near edge spectra of the Sr_2MnSbO_6 compounds along with some standards and previously studied compounds are shown in Fig. 3b. The elemental-Sb-L_1 spectrum manifests a broad peak due to 2*s*-core transitions into the three empty 5*p* states (as always a step-feature due to the onset of 2*s* to continuum transitions is also present). The Sb^{3+} standard Sb_2O_3 spectrum shows a dramatic chemical shift to higher energy, an increase in the intensity and narrowing (in energy) of the WL 5*p* feature. The increase in intensity is consistent with the greater number of 5*p*-holes, and the narrowing is consistent with the more localized atomic character in the higher valance state. The centrum of the WL peak-feature of the Sb^{5+} standard, Sb_2O_5 spectrum exhibits a clear shift to higher energy and the development of a higher energy second peak. The Sb-L_1 spectra of both the ordered and disordered Sr_2MnSbO_6 compounds are remarkable in that their WL-features are quite narrow and strongly shifted to higher

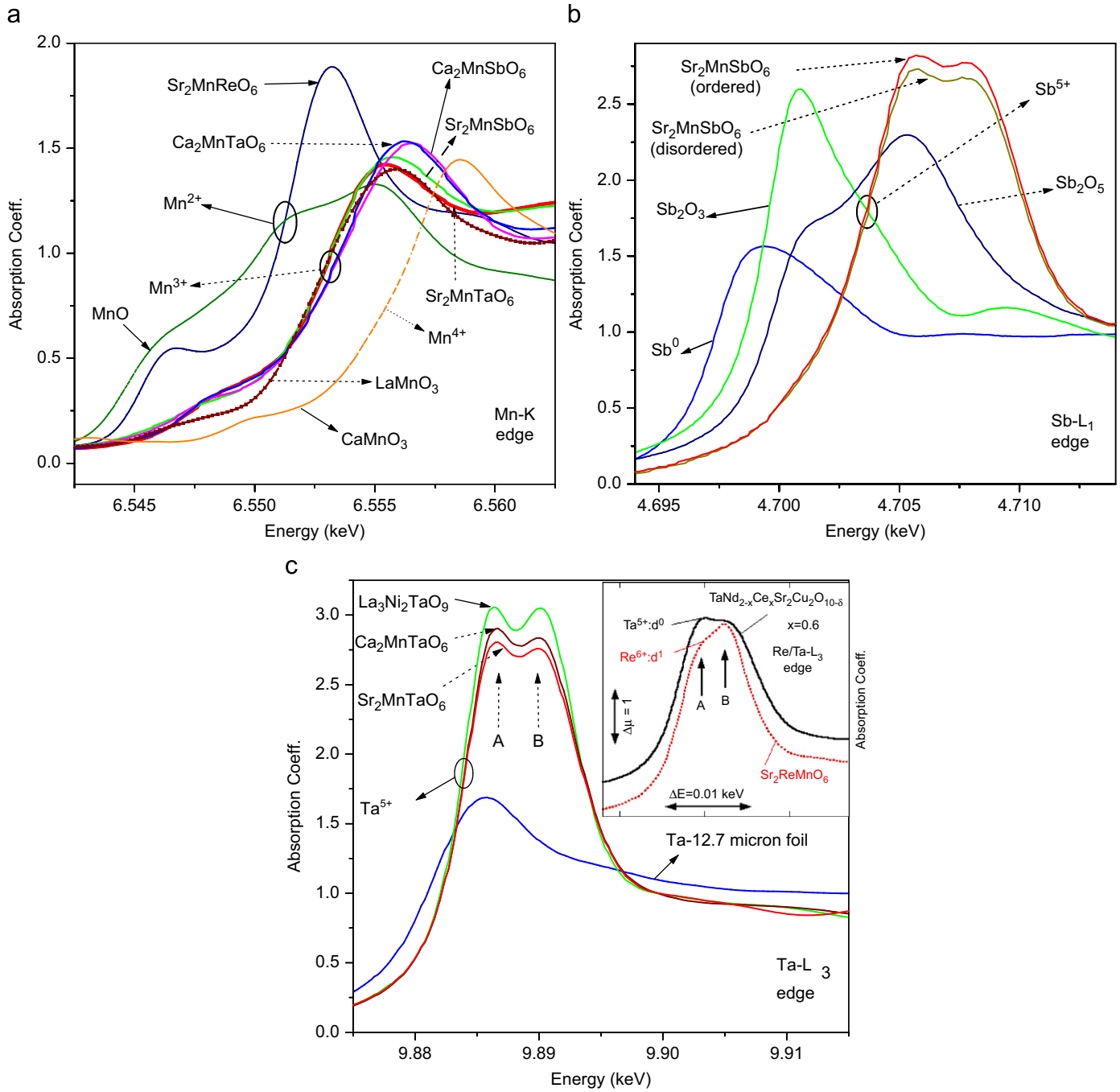

Fig. 3. X-ray absorption spectroscopic data for $A_2MnB'O_6$ (A = Ca, Sr; B = Sb, Ta) double perovskites along with representative standards at the (a) Mn-K, (b) Sb-L_1 and (c) Ta-L_3 edges.

energy. Indeed, it would appear that Sr_2MnSbO_6 constitutes a better pure Sb^{5+} XAS standard than does the binary oxide. The Sb^{5+} valence state in Sr_2MnSbO_6 is abundantly clear from the Sb-L_1 edge measurements.

The Ta-L_3 edges of A_2MnTaO_6 (A = Ca, Sr) along with various Ta compounds are shown in Fig. 3c and its inset. The $L_{2,3}$ near edge WL-features of 5d-transition metal, T(5d), compounds are due to transitions from the 2p to 5d states of the transition metal. In the octahedral ligand field of perovskite-based materials the 5d states are split into a six-fold degenerate t_{2g} ground state below a four-fold degenerate e_g state. The L_3 edge WL-feature of two such 5d-compounds, in the inset of Fig. 3c, clearly manifest overlapping A- and -B-features associated with the t_{2g} and e_g final states, respectively. It should be noted that the relative intensity of the A-feature decreases as the number of empty t_{2g} states decreases (i.e. as the electron count increases from d^0 to d^1). Thus the relative A to B feature intensity can be used to track the d-electron/hole count in such T(5d) compounds.

Turning to the main portion of Fig. 3c, the A/B-feature spectral structure is apparent in the A_2MnTaO_6 double perovskite spectra. Moreover, the relative A–B feature intensity in these compounds is consistent with the Ta^{5+}-d^0 configuration. The L_3 edge of $La_3Ni_2TaO_9$ compound is included here because it serves as another example of Ta^{5+}-d^0 configuration compound with the largest and best resolved T(5d) A/B-feature spectral splitting observed by the authors to date. Thus the unambiguous 5+

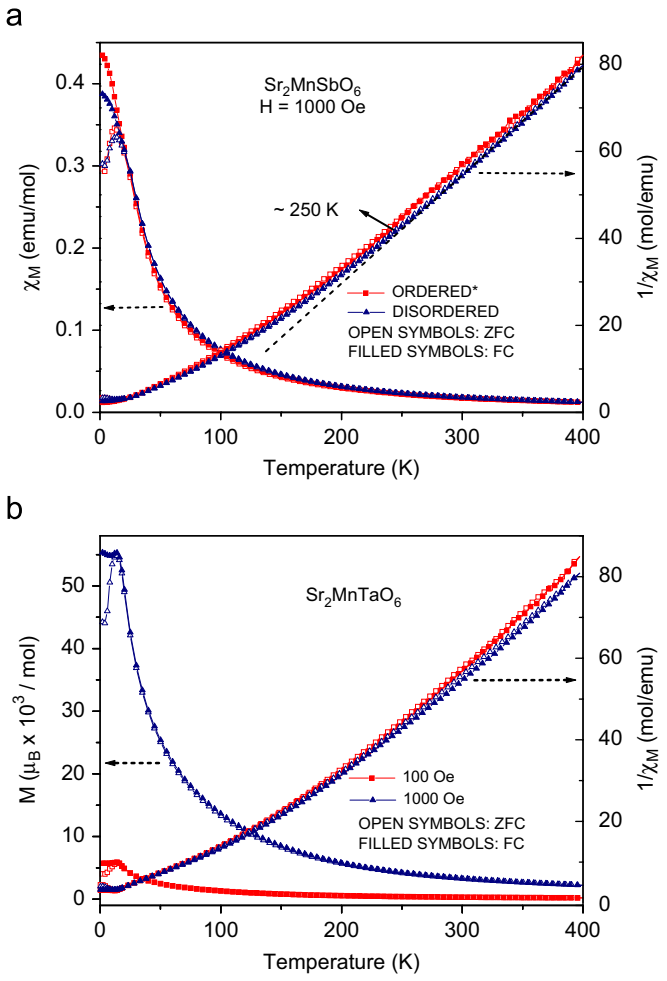

Fig. 4. Magnetization and inverse molar susceptibility ($1/\chi$) versus temperature plots for (a) ordered and disordered Sr_2MnSbO_6 and (b) Sr_2MnTaO_6.

valence state assignment for Ta and Sb (see above) follows from the XAS results on all of the $A_2MnB'O_6$ (A = Ca, Sr; B' = Sb, Ta) compounds.

3.3. Magnetic properties

The dc molar magnetization data for Sr_2MnSbO_6 as a function of temperature and at a magnetic field of 1000 Oe are shown in Fig. 4a for both the ordered and the disordered variants. The ZFC and FC data coincide down to 25 K below which they deviate from each other. Both samples showed a magnetic transition/glassy freezing (T^*) at about the same temperature (~16 K). An inspection of the FC data indicates that a somewhat higher value for the magnetization is obtained in case of the ordered sample as compared to the disordered Sr_2MnSbO_6. A Curie–Weiss ([$\chi = C/(T-\theta_W)$]) fit of the high temperature (300–400 K) inverse molar susceptibility data (Fig. 4a) for both samples gives positive Weiss constants (θ_W) indicating ferromagnetic correlations. However, we find that the value of θ_W (Table 3) for the disordered sample is higher as compared to the ordered variant. This would be consistent with Mn-clusters being the cause of the ferromagnetic correlations. An estimation of effective paramagnetic moment from the linear fit provides $\mu_{eff} = 5.68$ and $5.59\,\mu_B$ for the ordered and the disordered samples, respectively. The experimental values of μ_{eff} are significantly higher than $\mu_{cal} = 4.90\,\mu_B$ for Mn^{3+}:d^4 HS configuration. The Sr_2MnTaO_6 compound showed a very similar magnetic behavior with a T^* of ~14 K (Table 3). The temperature at

Table 3
Effective paramagnetic moment (μ_{eff}), Weiss constant (θ_W) and magnetic transition/glassy temperatures (T^*) in 0.1 T magnetic field for $A_2MnB'O_6$ (A = Ca, Sr; B' = Sb, Ta) double perovskites

Compound	μ_{eff}[a] (μ_B/f.u.)	θ_W (K)	T^* (K)
Sr_2MnSbO_6-ordered	5.68	71	16
Sr_2MnSbO_6-disordered	5.59	90	16
Sr_2MnTaO_6	5.39	107	14
Ca_2MnSbO_6	5.22	66	14
Ca_2MnTaO_6	5.04	64	12

[a] $\mu_{cal} = 4.90\,\mu_B$ (assuming Mn^{3+}:d^4 HS configuration).

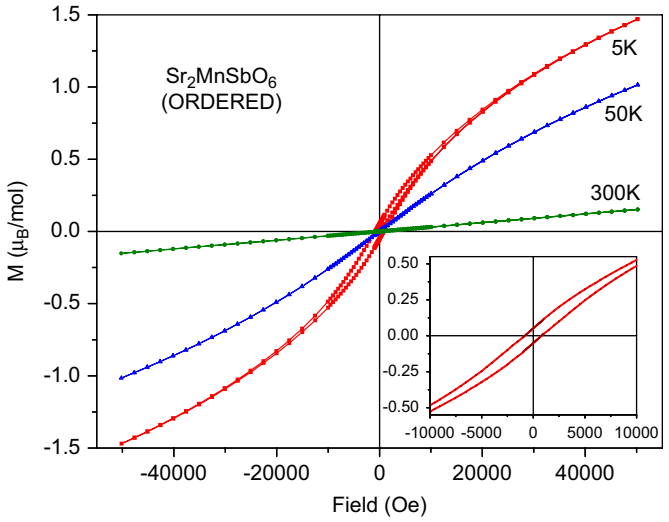

Fig. 5. Field dependence of magnetization data for ordered Sr_2MnSbO_6 at different temperatures.

which the ZFC and FC curves diverge in case of the previously reported Sr_2MnTaO_6 has been attributed to a freezing temperature (T_f), which in our case coincides with T^* [9].

The M vs. H plots for the ordered Sr_2MnSbO_6 are shown in Fig. 5. While the magnetization data at 300 K shows pure paramagnetic behavior, at 50 K the data indicate Brillouin-like curvature with no hysteresis. This is consistent with ferromagnetically coupled clusters [22]. At 5 K, the magnetization data show a hysteresis loop (inset of Fig. 5) with a Brillouin-like curvature feature up to 5 T, supporting significant ferromagnetic correlations in the ordered/glassy state.

The effective magnetic moments, Weiss temperatures and transition/glassy freezing temperatures (T^*) for the Ca-compounds are listed in Table 3. An analysis of the magnetic data (Fig. 6) for the Ca-analogs showed very similar behavior. However, a comparison of their magnetic behavior indicates that the Sr-analogs show non-linearity in their inverse susceptibility data starting below 250 K while the Ca-analogs demonstrate paramagnetic behavior down to ~180 K. In all the cases, a positive Weiss temperature indicates predominance of ferromagnetic interactions. Considering the inherent disorder present in all these materials, the behavior could be attributed to formation of ferromagnetic-like clusters in these systems [22].

A comment on the enhanced CW moment with respect to theoretical Mn^{3+} value in these compounds is in order. In general the inverse susceptibility of these compounds at high temperatures shows a ferromagnetic CW–θ, which decreases continuously with decreasing temperature. A potential mechanism could be proposed for such a behavior. The substantial B^{5+}/Mn^{3+} valence

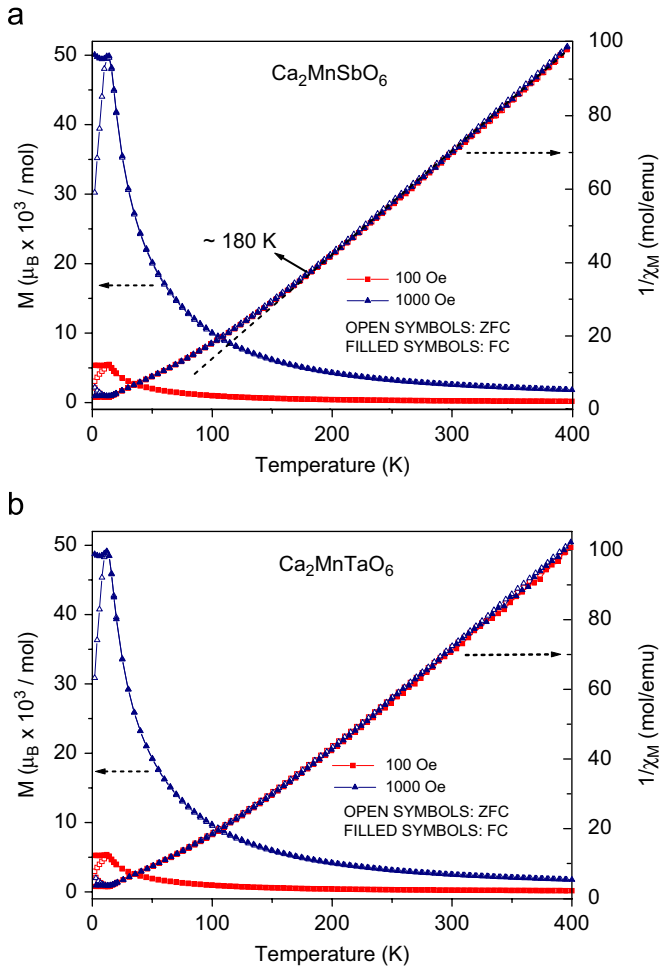

Fig. 6. Magnetization and inverse molar susceptibility ($1/\chi$) versus temperature plots for (a) Ca_2MnSbO_6 and (b) Ca_2MnTaO_6.

state difference and the disorder in these two species could reasonably be expected to create substantial variations in the local chemical potential at various Mn sites. These Mn sites/clusters with a local deviation from Mn^{3+} could interact via electron hopping yielding local ferromagnetic double exchange interactions. Indeed, such local hopping could be thermally activated facilitating an increased local ferromagnetic cluster interaction at high temperatures. The observed enhanced moment, ferromagnetic interactions which appear to weaken at lower temperatures and the cluster-type magnetism would appear to be consistent with this proposal.

4. Conclusions

We have synthesized $A_2MnB'O_6$ (A = Ca, Sr; B = Sb, Ta) double perovskites and investigated their structure and properties with powder X-ray diffraction, X-ray absorption spectroscopy and magnetization studies. Rietveld refinements of the powder X-ray diffraction data indicated significant ordering of the B-site cation only in the case of Sr_2MnSbO_6. The substantial order of Mn/Sb in Sr_2MnSbO_6 compared to the near complete disorder of Mn/Ta in Sr_2MnTaO_6 has been attributed to significantly larger difference in the effective ionic radii of Mn^{3+}–Sb^{5+} as compared to Mn^{3+}–Ta^{5+}. X-ray absorption spectroscopic data demonstrated the presence of Mn^{3+} and Sb^{5+}/Ta^{5+} in all the double perovskites studied here. All the compounds showed very similar magnetic behavior with positive Weiss temperatures signifying ferromagnetic correlations. The Brillouin-like feature in the magnetization data for Sr_2MnSbO_6 indicated formation of ferromagnetic-like clusters in the system.

Acknowledgements

This work was supported by the National Science Foundation through NSF-DMR-0233697, NSF-DMR-0541911.

References

[1] (a) F.K. Patterson, C.W. Moeller, R. Ward, Inorg. Chem. 2 (1963) 196;
(b) T. Nakagawa, J. Phys. Soc. Jpn. 24 (1968) 806;
(c) J. Longo, R. Ward, J. Am. Chem. Soc. 83 (1961) 2816;
(d) A.W. Sleight, J.F. Weiher, J. Phys. Chem. Solids 33 (1972) 679;
(e) M. Abe, T. Nakagawa, S. Nomura, J. Phys. Soc. Jpn. 35 (1973) 1360;
(f) K.-I. Kobayashi, H. Sawada, K. Terakura, Y. Tokura, Nature (London) 395 (1998) 677;
(g) K.-I. Kobayashi, T. Kimura, H. Sawada, K. Terakura, Y. Tokura, Phys. Rev. B 59 (1999) 11159;
(h) J. Gopalakrishnan, A. Chattopadhyay, S.B. Ogale, T. Venkatesan, R.L. Greene, A.J. Millis, K. Ramesha, B. Hannoyer, G. Marest, Phys. Rev. B 62 (2000) 9538.
[2] (a) M.T. Anderson, K.B. Greenwood, G.A. Taylor, K.R. Poeppelmeier, Prog. Solid State Chem. 22 (1993) 197;
(b) F. Galasso, L. Katz, R. Ward, J. Am. Chem. Soc. 81 (1959) 820;
(c) F. Galasso, W. Darby, J. Phys. Chem. 66 (1962) 131.
[3] (a) P. Woodward, R.-D. Hoffmann, A.W. Sleight, J. Mater. Res. 9 (1994) 2118;
(b) T. Shimada, J. Nakamura, T. Motohashi, H. Yamauchi, M. Karppinen, Chem. Mater. 15 (2003) 4494.
[4] F. Galasso, F.C. Douglas, R. Kasper, J. Chem. Phys. 44 (1966) 1672.
[5] H.-Y. Hwang, S.-W. Cheong, N.P. Ong, B. Batlogg, Phys. Rev. Lett. 77 (1996) 2041.
[6] N.S. Rogado, J. Li, A.W. Sleight, M.A. Subramanian, Adv. Mater. 17 (2005) 2225.
[7] M.W. Lufaso, P.M. Woodward, J. Goldberger, J. Solid State Chem. 117 (2004) 1651.
[8] M. Cheah, P.J. Saines, B.J. Kennedy, J. Solid State Chem. 179 (2006) 1775.
[9] M. Valldor, S. Esmaeilzadeh, M. Andersson, A. Morawski, J. Magn. Magn. Mater. 299 (2006) 161.
[10] V. Poltavets, K. Vidyasagar, M. Jansen, J. Solid State Chem. 177 (2004) 1285.
[11] S. Kato, T. Sakamoto, N. Watanabe, M. Sugai, Y. Ohshima, H. Takizawa, M. Shimada, Mater. Lett. 21 (1994) 101.
[12] H.M. Rietveld, J. Appl. Crystallogr. 2 (1969) 65.
[13] J. Rodriguez-Carvajal, Physica B 192 (1993) 55.
[14] J.M. Tranquada, S.M. Heald, A.R. Moodenbaugh, G. Liang, M. Croft, Nature (London) 337 (1989) 720.
[15] M. Croft, D. Sills, M. Greenblatt, C. Lee, S.-W. Cheong, K.V. Ramanujachary, D. Tran, Phys. Rev. B 55 (1997) 8726.
[16] (a) T. Guo, M. DenBoer, Phys. Rev. B 31 (1985) 6233;
(b) Y. Jeon, J. Chen, M. Croft, Phys. Rev. B 50 (1994) 6555.
[17] R.D. Shannon, Acta Crystallogr. A 32 (1976) 751.
[18] A.M. Glazer, Acta Crystallogr. B 28 (1972) 3384.
[19] V.K. Pecharsky, P.Y. Zavalij, Fundamentals of Powder Diffraction and Structural Characterization of Materials, first ed, Springer, 2003, p. 227.
[20] P.M. Woodward, Acta Crystallogr. B 53 (1997) 32.
[21] C.J. Howard, H.T. Stokes, Acta Crystallogr. B 54 (1998) 782.
[22] H. Woo, T.A. Tyson, M. Croft, S.-W. Cheong, J. Phys.: Condens. Matter 16 (2004) 2689.